European Journal of Chemistry 2 (2) (2011) 136-145

European Journal of Chemistry

Journal homepage: www.eurjchem.com

Theoretical and experimental studies on 2-(2-methyl-5-nitro-1-imidazolyl)ethanol

Sirukarumbur Panduranga Vijaya Chamundeeswari[a], Emmanuel Rajan James Jebaseelan Samuel[a] and Namadevan Sundaraganesan[b,*]

[a] *Photonics Division, School of Advanced Sciences, Vellore Institute of Technology University, Vellore, 632014, Tamilnadu, India*
[b] *Department of Engineering Physics, Annamalai University, Annamalai Nagar Chidambaram, 608002, India*

**Corresponding author at: Department of EngineeringPhysics, Annamalai University, Annamalai Nagar Chidambaram, 608002, India. Tel.: +91.9442068405; fax: +91.4144.238145. E-mail address: sundaraganesan_n2003@yahoo.co.in (N. Sundaraganesan).*

ARTICLE INFORMATION

Received: 16 June 2010
Received in revised form: 10 October 2010
Accepted: 14 November 2010
Online: 30 June 2011

KEYWORDS

Vibrational spectra
NBO analysis
TD-DFT
UV spectra
NMR
Metronidazole

ABSTRACT

In this work, we report a combined experimental and theoretical study on molecular structure, vibrational spectra, natural bond orbital (NBO) and UV spectral analysis of [2-(2-methyl-5-nitro-1-imidazolyl) ethanol] (Metronidazole-MTD). The FT-IR solid phase (4000-400 cm^{-1}) liquid phase, and FT-Raman spectra (3500-50 cm^{-1}) of MTD were recorded. The molecular geometry, harmonic vibrational frequencies and bonding features of MTD in the ground state have been calculated using the density functional method B3LYP with 6-311G(d,p) as basis set. The assignments of the vibrational spectra have been carried out with the help of the Gauss view program package. Stability of the molecule arising from hyperconjugative interactions and charge delocalization have been analyzed using natural bond orbital analysis. The results show that charge in electron density (ED) in the σ* and π* antibonding orbitals and second order stabilization energies E^2 confirms the occurrence of Intramolecular Charge Transfer (ICT) within the molecule. The UV spectrum was measured in ethanol solution. The energy and oscillator strength calculated by Time-Dependent Density Functional Theory (TD-DFT) results complement the experimental findings. The calculated HOMO and LUMO energies show that charge transfer occurs within the molecule. The ^1H and ^{13}C nuclear magnetic resonance (NMR) chemical shifts of the molecule were calculated by the Gauge Independent Atomic Orbital (GIAO) method and compared with experimental results. Finally the results of calculations were applied to simulate Infrared and Raman spectra of the title compound which show good agreement with observed spectra.

1. Introduction

Metronidazole (MTD) is an antibiotic used to treat different kinds of infections. It is available in oral, rectal, vaginal and topical preparations. Metronidazole is commonly used for vaginal infections for which pregnant women can require treatment. It has been available in the market for more than 40 years. Another name for metronidazole is Flagyl [1]. It is a highly effective drug for the treatment of intestinal amoebiasis, giardiasis, trichomoniasis and for the prevention of other mechanism of this drug, it is accepted that its reduced form is the one that really provokes the biochemical damages resulting in foreign cell destruction producing selective toxicity for anaerobic or microaerofilic microorganism and hypoix cells [2]. It is known that the oral treatment with metronidazole may cause a group of side-effects associated with strong gastrointestinal disturbances (i.e. gastritis, nausea and vomiting). These side effects can eventually be strong enough to have the treatment cancelled. Due to its effectiveness metronidazole is considered as an election drug for several pathologies [2]. To the best of our knowledge neither IR and Raman spectra nor the quantum mechanical calculations for MTD molecule have been reported so far, and only XRD analysis has been done by Blaton *et al.* [3]. NIR-FT-Raman spectroscopy combined with quantum chemical computations has been recently used as an effective tool in the vibrational analysis of drug molecules [4], biological compounds [5] and natural products [6], since fluorescence-free Raman spectra and the computed results can help unambiguous identification of vibrational modes as well as the bonding and structural features of complex organic molecular systems.

In the present study, FT-IR, FT-Raman and UV spectral investigation of MTD, have been performed using density functional theory (DFT) for the first time. The redistribution of electron density (ED) in various bonding and antibonding orbitals and E^2 energies have been calculated by natural bond orbital (NBO) analysis using DFT method to give clear evidence of stabilization originating from the hyperconjugation of various intramolecular interactions. The UV spectroscopic studies along with HOMO, LUMO analysis have been used to explain information regarding charge transfer within the molecule.

2. Experimental

The compound Metronidazole was purchased from Sigma-Aldrich Chemical Company (USA) with a stated purity of greater than 97% and it was used as such without further purification. The FT-IR spectrum of this solid sample was recorded in the region 400–4000 cm^{-1} on IFS 66V

ISSN 2153-2249 (Print) / ISSN 2153-2257 (Online)
DOI:10.5155/eurjchem.2.2.136-145.169

spectrophotometer using KBr pellet technique in room temperature. The FT-IR spectra of solution was also recorded in the range 400-4000 cm^{-1} in the same instrument. Chloroform was used as solvent to get the solution spectra. The FT-Raman spectrum of solid MTD has been recorded using 1064 nm line of Nd:YAG laser as excitation wavelength in the region 50-3500 cm^{-1} on a Thermo Electron Corporation model Nexus 670 spectrophotometer equipped with FT-Raman module accessory. The measured FT-IR and FT-Raman spectra along with theoretically constructed spectra are shown in Figure 1 and 2.

The ^{13}C NMR and ^{1}H NMR spectra were recorded on Bruker Avance 300 MHz FT-NMR spectrometer, $CDCl_3$ was used as a solvent and TMS as an internal standard. The measured ^{1}H and ^{13}C NMR spectra are shown in Figure 3 and 4. The ultraviolet absorption spectra of MTD is examined in the range 200-500 nm using the Shimadzu UV-2401PC, UV-VIS recording spectrometer. The UV pattern is taken from a 10^{-5} molar solution of MTD, dissolved in ethanol as shown in Figure 5.

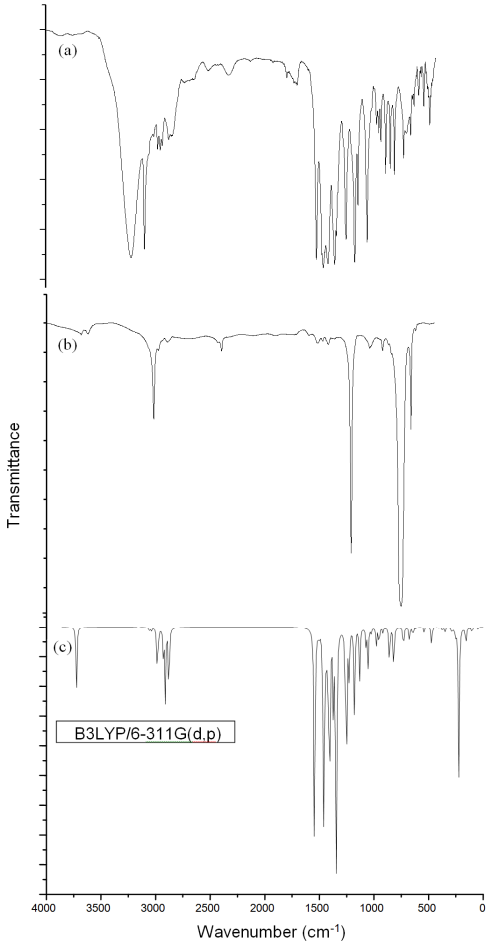

Figure 1. Comparison of FT-IR spectrum (a) solid (b) metronidazole + (ethanol) (c) theoretical FT-IR spectrum.

2.1. Computational details

To meet the requirements of both accuracy and computing economy, theoretical methods and basis sets should be considered. Density functional theory (DFT) has been proved to be extremely useful in treating electronic structure of molecules. The basis set 6-311G(d,p) was used as an effective and economical level to study fairly large organic molecules. Based on the points, the density functional three-parameter hybrid model (DFT/B3LYP) at the 6-311G(d,p) basis set level was adopted to calculate the properties of the studied molecule in the present work. All the calculations were performed using the Gaussian 03W program package [7] with the default convergence criteria, without any constraint on the geometry [8]. Geometries of the model MTD have been first optimized with full relaxation on the potential energy surfaces at HF/6-311G(d,p) level and the resultant geometries have been used as inputs for further calculations at DFT(B3LYP) level. The assignments of the calculated wavenumbers are aided by the animation option of Gauss View 3.0 graphical interface from the Gaussian program which gives a visual presentation of the shape of the vibrational modes [9].

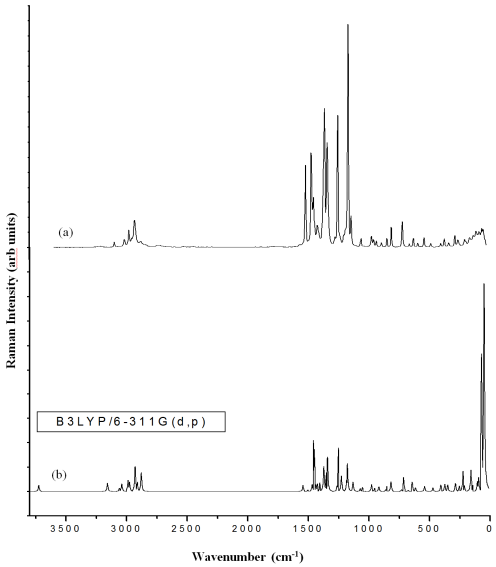

Figure 2. FT-Raman spectrum (a) experimental (b) theoretical of metronidazole.

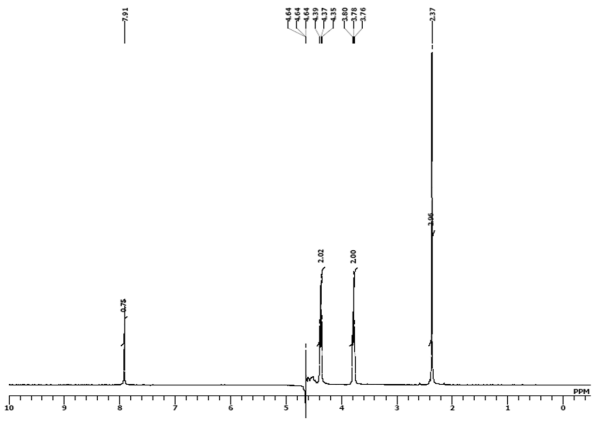

Figure 3. ^{1}H NMR spectrum of metronidazole.

The natural bonding orbital (NBO) calculations [10] were performed using NBO 3.1 program as implemented in the Gaussian 03W [7] package at the above said level in order to understand various second order interactions between the filled orbitals of one subsystem and vacant orbitals of another subsystem, which is a measure of the intermolecular delocalization or hyper conjugation.

Finally the geometry of the title compound, together with that of DMSO is fully optimized. ^{1}H and ^{13}C NMR chemical shifts are calculated with GIAO approach [11,12] by applying B3LYP/6-311G(d,p) method. The theoretical NMR ^{1}H and ^{13}C

chemical shift values were obtained by subtracting the GIAO calculation [13,14]. ^{13}C and ^{1}H isotropic magnetic shielding (IMS) of any X atom (carbon or hydrogen) were made according to the value TMS. $CS_x = IMS_{TMS} - IMS_x$.

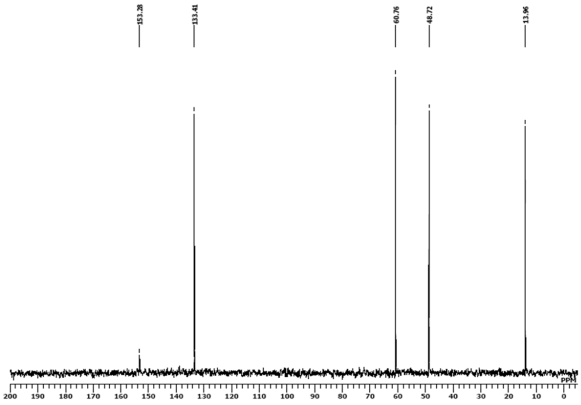

Figure 4. ^{13} C NMR spectrum of metronidazole.

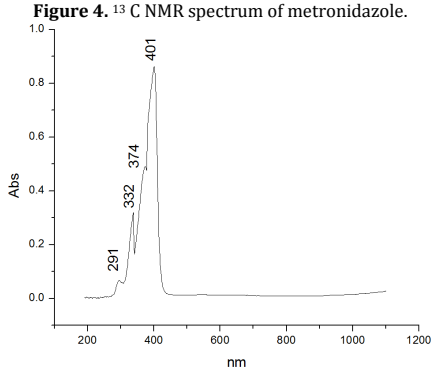

Figure 5. UV-Visible spectrum of metronidazole.

2.2. Prediction of Raman intensities

The Raman activities (S_i) calculated with the Gaussian 03 program [7] are converted to relative Raman intensities (I_i) using the following relationship derived from the intensity theory of Raman scattering [15,16].

$$I_i = \frac{f(v_o - v_i)^4 S_i}{v_i[1 - \exp(-hcv_i / kt)]} \quad (1)$$

where v_o is the exciting frequency in cm^{-1}, v_i the vibrational wavenumber of the i^{th} normal mode, h, c and k are fundamental constants, and f is a suitably chosen common normalization factor for all peak intensities. For the simulation of calculated FT-Raman spectra have been plotted using pure Lorentzian band shape with a bandwidth of Full Width and Half Maximum (FWHM) of 10 cm^{-1} as shown in Figure 2.

3. Results and discussions

3.1. Geometric structure

The optimized structure parameters of MTD calculated by DFT level show strong hydrogen bonding, which is in Table 1 in accordance with the atom numbering scheme given in Figure 6a. From Table 1, it can be noted that there are some deviations when compared to the single crystal XRD data [3], and these differences are probably due to the intermolecular interactions in the crystalline state. The computed bond lengths, bond angles and torsional angles are in reasonable agreement with the corresponding experimental values. Metronidazole crystallizes in space group P21/c, with four molecules per unit cell (Z = 4). From the single crystal XRD data [3] it is observed that the crystal belongs to monoclinic system with the following cell dimensions: a = 7.034(2) Å, b = 8.725(3) Å and c = 12.818(3) Å. According to the crystal data, the C(1)-NO_2 group is planar and makes an angle of 4.3° with the imidazole plane. Our theoretical calculation by B3LYP method also predicted the same behavior as evident from the torsional angle of N4-C1-N11-O13 = -168.58°. Molecules are strongly hydrogen bonded with a symmetrically related neighbor O(42)-H(43)....N(6); O(20)-N(6)=2.816(2) Å, H(21)....N(6)=1.98(2) Å. The computed dimer parameters (intermolecular hydrogen bonding) by B3LYP method shows good agreement with X-ray data. From the theoretical values we can find that most of the optimized bond lengths are slightly smaller than the experimental values.

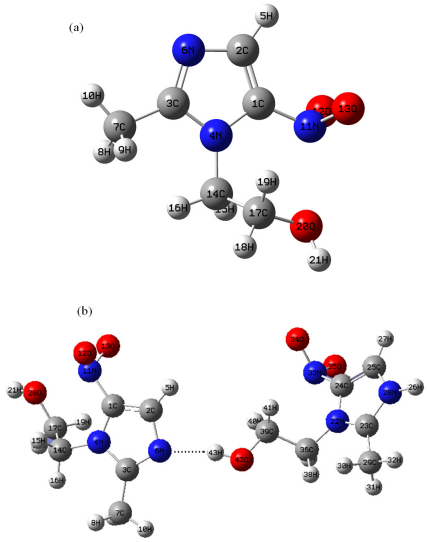

Figure 6. (a) Molecular structure and atom numbering scheme adopted in this study for metronidazole (b) dimer structure of metronidazole.

The bond lengths in the heterocyclic five membered ring are comparable with the X-ray data of metronidazole [3]. The C(1)-N(11) bond distance of 1.43 Å calculated by B3LYP method is just 0.16 Å lower than the X-ray data [3]. It is interesting to note that nitro groups in 5-bromo-2-nitropyridine and 2-nitropyridine [17] molecule, one N-O bond length (1.227 Å) was longer than the other N-O bond length (1.213 Å). This effect can be attributed to the repulsion between the lone pair on the oxygen atom and the electron pair on the nitrogen atom. Similar trend is not observed in our title molecule of NO_2 group. The calculated bond length of N(11)-O(12) and N(11)-O(13) is equal and is 1.23 Å by B3LYP method.

3.2. Hydrogen bonding

The crystal structure shows the presence of intermolecular hydrogen bond interaction in MTD as shown in Figure 6b. In our present study the hydrogen bond analysis is carried out by B3LYP method. The weak hydrogen bond type of interaction between O42-H43.....N6 is calculated, the distance between O42.....N6 is about 3.071 Å, respectively and are well within the range < 3.0 Å for hydrogen interaction [18].

3.3. NBO analysis

NBO analysis provides the most accurate possible 'natural Lewis structure' picture of ø, because all orbital details are mathematically chosen to include the highest possible percentage of the electron density.

Table1. Geometrical parameters optimized in MTD.

Parameters	B3LYP/ 6-311G(d,p)	Experimental XRD [a]	Parameters	B3LYP/ 6-311G(d,p)	Experimental XRD [a]
Bond length (Å)			**Bond angle (°)**		
C1-C2	1.37	1.356(2)	C2-N6-C3	106.06	106.2(1)
C1-N4	1.39	1.383(2)	C3-C7-H8	111.90	
C1-N11	1.43	1.414(2)	C3-C7-H9	112.32	
C2-H5	1.08	0.94(2)	C3-C7-H10	107.72	
C2-N6	1.36	1.359(2)	H8-C7-H9	107.79	113.0(1)
C3-N4	1.37	1.351(2)	H8-C7-H10	108.57	105.2(1)
C3-N6	1.33	1.334(2)	C1-N11-O12	118.89	
C3-C7	1.49	1.476(2)	C1-N11-O13	116.36	
N4-C14	1.47	1.475(2)	O12-N11-O13	124.72	
C7-H8	1.09	0.99(2)	N4-C14-H15	107.89	
C7-H9	1.09	0.95(2)	N4-C14-H16	107.83	
C7-H10	1.09	0.95(2)	N4-C14-C17	112.41	
N11-O12	1.23	1.226(2)	H15-C14-H16	109.04	107.0(1)
N11-O13	1.23	1.221(2)	H15-C14-C17	109.85	111.0(1)
C14-H15	1.09	0.99(2)	H16-C14-C17	109.74	112.0(1)
C14-H16	1.09	0.99(2)	C14-C17-H18	107.78	111.0(1)
C14-C17	1.53	1.510(2)	C14-C17-H19	109.86	111.5(1)
C17-H18	1.10	0.99(2)	C14-C17-O20	107.89	
C17-H19	1.10	0.99(2)	H18-C17-H19	108.10	108.0(1)
C17-O20	1.42	1.410(2)	H18-C17-O20	111.74	113.0(1)
O20-H21	0.96	0.84(2)	H19-C17-O20	111.40	107.0(1)
Bond angle (°)			C17-O20-H21	108.94	110.0(1)
C2-C1-N4	106.87	107.6(1)	**Dihedral Angle (°)**		
C2-C1-N11	127.10	126.9(1)	N4-C1-N11-O12	13.45	-3.4(3)
C4-C1-N11	125.71		N4-C1-N11-O13	-168.58	-176.1(2)
C1-C2-H5	127.08	126.0(1)	N6-C3-N4-C14	171.16	
C1-C2-N6	109.74	109.1(1)	C7-C3-N4-C1	-179.42	
H5-C2-N6	123.16	125.0(1)	C7-C3-N4-C14	-9.47	
N4-C3-N6	112.17	111.5(1)	N4-C3-N6-C2	-1.01	
N4-C3-C7	123.88	124.4(1)	C7-C3-N6-C2	179.63	
N6-C3-C7	123.95	124.0(1)	C4-C3-C7-H8	-58.06	
C1-N4-C3	105.15	105.5(1)	C4-C3-C7-H9	63.35	
C1-N4-C14	128.36		C1-N4-C14-C17	82.85	82.6(2)
C3-C4-C14	125.60	125.5(1)	N4-C14-C17-O20	-62.75	61.2(2)

[a] X-ray data taken from Ref. [10].

A useful aspect of the NBO method is that it gives information about interactions in both filled and virtual orbital spaces that could enhance the analysis of intra- and intermolecular interactions.

The second order Fock matrix was carried out to evaluate the donor–acceptor interactions in the NBO analysis [19]. The interactions result is a loss of occupancy from the localized NBO of the idealized Lewis structure into an empty non-Lewis orbital. For each donor (i) and acceptor (j), the stabilization energy E(2) associated with the delocalization i → j is estimated as

$$E_2 = \Delta E_{ij} = q_i \frac{F(i,j)^2}{\varepsilon_j - \varepsilon_i} \quad (2)$$

where q_i is the donor orbital occupancy, ε_i and ε_j are diagonal elements and F(i,j) is the off diagonal NBO Fock matrix element. Natural bond orbital analysis provides an efficient method for studying intra- and intermolecular bonding and interaction among bonds and also provides a convenient basis for investigating charge transfer or conjugative interaction in molecular systems. Some electron donor orbital, acceptor orbital and the interacting stabilization energy resulting from the second-order micro-disturbance theory are reported [20,21].

The larger the *E*(2) value, the more intensive is the interaction between electron donors and electron acceptors, i.e. the more donating tendency from electron donors to electron acceptors the greater the extent of conjugation of the whole system. Delocalization of electron density between occupied Lewis-type (bond or lone pair) NBO orbitals and formally unoccupied (antibond or Rydgberg) non-Lewis NBO orbitals correspond to a stabilizing donor–acceptor interaction. NBO analysis has been performed on the molecule at the DFT level in order to elucidate the intramolecular, rehybridization and delocalization of electron density within the molecule.

The intramolecular interaction is formed by the orbital overlap between bonding (C-C), (C-N) and (C-C), (C-N) antibond orbital which results in intramolecular charge transfer (ICT) causing stabilization of the system. These interactions are observed as increase in electron density (ED) in C-C, C-N antibonding orbital that weakens the respective bonds. The electron density of five conjugated single as well as double bond of imidazole ring (~1.9 e) clearly demonstrates a strong delocalization for MTD molecules. The strong intramolecular hyperconjugative interaction of the σ and π electrons of C-C and C-N to the anti C-C, C-N bond of the ring leads to stabilization of some part of the ring as evident from Table 2. The intramolecular hyperconjugative interaction of the σ (C1-C2) distributes to σ* (C1-N11), (N4-C14) leading to stabilization of 4 kJ/mol. This enhances further conjugation with antibonding orbital of π* (C3-N6) which leads to strong delocalization of 12.61 kJ/mol, respectively. The same kind of interaction is calculated in the C3-N6, N11-O12, and N11-O13 bond as shown in Table 2. The most interaction energy, related to the resonance in the molecule, is electron donating from the LP(1)N4 to the anti-bonding acceptor π* (C1-C2), (C3-N6) of the imidazole ring which leads to moderate stabilization energy of ~ 40 kJ/mol as shown in Table 2. The σ* (N11-O12) of the NBO conjugated with π* (N11-O13), π* (N11-O12) resulting in a stabilization of 69.21 and 60.85 kJ/mol respectively as shown in Table 2. The π* (N11-O12) of the NBO orbital further conjugate with π* (N11-O13) resulting in an enormous stabilization of 15787.09 kJ/mol, respectively.

Table 2. Second order perturbation theory analysis of Fock matrix in NBO basis for MTD.

Donor (i)	Type	ED/e	Acceptor (j)	Type	ED/e	E(2)[a](KJ/mol)	E(j)-E(i)[b](a.u)	F(i,j)[c] (a.u)
C1-C2	σ	1.968	C1-N11	σ*	0.07	2.48	0.98	0.04
			N4-C14	σ*	0.03	4.91	1.01	0.06
	π	1.845	C3-N6	π*	0.02	12.61	0.26	0.06
C1-N4	σ	1.982	C3-N4	σ*	0.04	2.27	1.23	0.05
			C3-C7	σ*	0.02	3.20	1.17	0.06
			N4-C14	σ*	0.03	1.59	1.11	0.04
C2-H5	σ	1.984	C1-N4	σ*	0.04	2.71	0.95	0.05
C2-N6	σ	1.965	C1-N11	σ*	0.07	8.11	0.98	0.08
			C3-C7	σ*	0.02	5.55	1.07	0.07
			C3-N4	σ*	0.04	2.52	1.22	0.05
			C1-N11	σ*	0.07	4.64	1.08	0.06
C3-N6	σ	1.982	N4-C14	σ*	0.03	4.14	1.07	0.06
	π	1.848	C1-C2	π*	0.34	19.75	0.29	0.07
C3-C7	σ	1.984	C1-N4	σ*	0.04	3.01	1.06	0.05
C7-H8	σ	1.979	C3-N6	σ*	0.02	3.50	0.52	0.04
C7-H9	σ	1.979	C3-N6	σ*	0.02	3.45	0.52	0.04
C7-H10	σ	1.984	C3-N4	σ*	0.04	5.51	0.95	0.07
N11-O12	σ	1.699	N11-O12	σ*	0.14	4.89	0.90	0.06
			N11-O12	π*	0.35	80.00	1.24	0.30
			N11-O13	σ*	0.14	29.00	0.90	0.14
			N11-O13	π*	0.36	86.23	1.25	0.31
			N11-O12	σ*	0.14	79.23	0.50	0.19
			N11-O12	π*	0.35	118.52	0.84	0.29
			N11-O13	σ*	0.14	50.42	0.50	0.15
			N11-O13	π*	0.35	257.36	0.85	0.42
N11-O13	σ	1.881	N11-O12	σ*	0.14	28.69	0.91	0.15
			N11-O12	π*	0.35	75.43	1.26	0.29
			N11-O13	σ*	0.14	72.37	1.27	0.29
			N11-O12	σ*	0.35	57.57	0.49	0.16
			N11-O12	π*	0.35	259.85	0.83	0.42
			N11-O13	σ*	0.14	72.80	0.49	0.18
			N11-O13	π*	0.35	123.71	0.84	0.29
N4	LP(1)	1.555	C1-C2	π*	0.02	33.55	0.28	0.09
			C3-N6	π*	0.02	48.10	0.26	0.10
C3-N6	π*	1.848	C1-C2	π*	0.02	65.73	0.02	0.05
N11-O12	π*	1.699	N11-O13	π*	0.36	69.21	0.35	0.28
			N11-O13	π*	0.36	15787.09	0.01	0.65
	σ*		N11-O12	π*	0.35	60.85	0.35	0.26

[a] E(2) means energy of hyper conjugative interaction (stabilization energy); [b] Energy difference between donor and acceptor i and j NBO orbitals; [c] F(i, j) is the Fock matrix element between i and j NBO orbitals.

3.4. Vibrational analysis

We performed a frequency calculation analysis and also recorded FT-IR and FT-Raman spectra based on the theoretically predicted wavenumbers by DFT (B3LYP) method which have been collected in Table 3, in order to obtain the spectroscopic signature of the MTD molecule. None of the predicted vibrational spectra has any imaginary frequency, implying that the optimized geometry is located at the minimum on the potential energy surface. We know that ab inito HF and DFT potentials systematically overestimate the vibrational wavenumbers. These discrepancies are corrected either by computing anharmonic corrections explicitly or by introducing scaled field [22] or directly scaling the calculated wavenumber with the proper scale factor [23]. In the study, we have used scaling factor of 0.967 for B3LYP/6-311G(d,p) method. After scaling with the scaling factor, the deviation from the experimental is less than 10 cm^{-1} with few exceptions. As per the theoretical calculations, studied MTD has assumed to possess a planar structure of C_s point group symmetry. On the basis of C_s symmetry the 57 fundamental vibrations of MTD can be distributed as 39 A' + 18 A''. All the vibrations are active in both IR and Raman.

3.4.1. O-H vibrations

The O-H group gives rise to three vibrations namely stretching, in-plane and out-of plane bending vibrations. The O-H group vibrations are likely to be the most sensitive to the environment, so they show pronounced shifts in the spectra of the hydrogen bonded species. The hydroxyl stretching vibrations are generally [24] observed in the region around 3500 cm^{-1}. In the case of the un-substituted phenols it has been shown that the frequency of O-H stretching vibration in the gas phase is 3657 cm^{-1}. Bands due to the O-H stretching are of medium to strong intensity in the infrared spectrum, although it may be broad. In Raman spectra the band is generally weak. Unassociated hydroxyl groups absorb strongly in the region 3670-3580 cm^{-1}. The band due to the free hydroxyl group is sharp and it is having strong intensity. For solid, liquids and concentrated solutions, a broad band of less intensity is normally observed [25,26]. In our present study the medium band observed in FT-IR (solid) at 3219 cm^{-1} is assigned to O-H stretching vibrations. The spectrum of dilute solution (chloroform) give the wavenumber at 3684 cm^{-1} corresponds to O-H vibration suggesting hydrogen bonding is absent in solution spectrum. A comparison of this band at 3219 cm^{-1} in FT-IR solid phase with that of the computed value at 3724 cm^{-1} shows positive deviation of ~494 cm^{-1}, which may be due to the presence of strong intermolecular hydrogen bonding (Mode no. 1).

The O-H in-plane bending vibration for phenol, in general, lies in the region 1150-1250 cm^{-1} and is not much affected due to hydrogen bonding unlike the stretching and out-of-plane bending wavenumber [27]. For our title molecule, the O-H in-plane bending vibration appears as a strong band at 1265 cm^{-1} in FT-IR spectrum, 1268 cm^{-1} as a very strong band in FT-Raman spectrum. The theoretically computed wavenumber at 1263 cm^{-1} (Mode no. 23) shows good agreement with experimental observations.

The O-H out-of-plane deformation vibration for phenol lies in the region 290-320 cm^{-1} for free O-H and in the region 517-710 cm^{-1} for associated O-H [28]. In both inter-molecular and intra-molecular associations, the wavenumber is at a higher value than free O-H. The wavennumber increases with hydrogen bond strength because of the large amount of energy required to twist the O-H bond [29].

Table 3. Vibrational wavenumbers obtained for MTD at B3LYP /6-311G(d,p) method [Harmonic frequency (cm^{-1}), IR_{int} ($Kmmol^{-1}$) R_{int} (arb units)].

Mode nos.	Experimental (cm^{-1})			Theoretical Wavenumber (cm^{-1})			Vibrational assignments
	FT-IR solid	FT-IR solution (Chloroform)	FT-Raman solid	B3LYP scaled	IR_{int}	R_{Int}	
1	3219m	3684w		3724	44.02	23.71	υ O-H
2				3157	0.88	32.12	υ C-H
3	3100m		3102w	3059	2.50	12.50	$υ_{asym}$ $C14H_2$
4		3019s	3019w	3039	2.97	32.84	$υ_{asym}$ CH_3
5	2982w		2983vw	2987	23.27	41.97	$υ_{sym}$ $C14H_2$
6		2967w		2975	15.64	38.42	$υ_{asym}$ CH_3
7	2956vw		2936m	2929	18.55	100.00	$υ_{sym}$ CH_3
8				2911	49.50	36.87	$υ_{asym}$ $C17H_2$
9	2850w	2890w	2885vw	2878	54.82	70.17	$υ_{sym}$ $C17H_2$
10	1535ms	1523w	1533vs	1544	206.79	22.98	$υ_{asym}$ NO_2
11	1486w	1478w	1486vs	1503	5.73	5.84	υC=N + υC-C
12	1473m		1467m	1468	26.65	28.34	δ $C17H_2$
13				1459	120.51	206.33	υC-C + δ$C14H_2$+ CH_3 asym.deform
14				1450	35.37	167.79	υC-C + υC=N
15			1435w	1437	11.78	28.15	CH_3 asym.deform
16	1429w	1426w		1424	35.27	29.76	δ $C14H_2$ + CH_3 asym.deform
17				1409	5.50	9.54	ω $C17H_2$+ β O-H
18				1406	138.07	33.56	δ $C14H_2$ + υC-N + CH_3 sym.deform
19	1369m		1377vs	1372	54.74	101.20	CH_3 sym.deform+ ω $C14H_2$
20			1355vs	1351	60.55	74.59	CH_3 sym.deform+ ω $C14H_2$
21				1345	22.97	22.16	ω $C14H_2$+ υC-N
22				1342	151.56	139.54	υ sym NO_2+ β C-H +ω $C14H_2$
23	1265s		1268vs	1263	32.81	22.37	β O-H + t $C14H_2$
24				1251	111.06	175.89	β C-H+ t $C17H_2$
25		1215vs		1227	31.64	58.11	t $C17H_2$+ β O-H
26	1187vs		1183vs	1183	10.46	44.35	ω $C17H_2$+ t $C14H_2$
27	1158m		1158w	1178	56.96	109.90	β C-N-C + β O-H+ t $C17H_2$
28				1131	35.70	35.65	β C-H
29	1074ms		1075vw	1072	12.72	11.39	υC-O
30		1046w		1053	27.40	15.55	ρ $C17H_2$+ β O-H
31	989w		990vw	1027	4.12	0.45	ρ CH_3
32	969w		973vw	978	13.49	28.06	ρ CH_3+ t $C14H_2$
33	949m		950vw	953	13.72	12.81	β C-N-C + β C-H + ρ $C17H_2$
34	907m	928w	908vw	918	3.77	18.99	υC14-C17 + β C-N-C
35	864m		863w	860	17.81	7.30	γ C-H
36				853	7.30	20.30	γ C-NO_2 + γ C-H
37	826vs		828w	818	35.24	38.67	δ NO_2
38	744m	759vs	737m	730	16.92	7.65	ω NO_2+ γ C-H
39	708m			714	0.28	58.18	υC-CH_3+ υN4-C14
40	679m	669m	680vw	675	9.29	5.23	γ N-C-N
41	647w	627w	646w	643	6.52	36.63	β N-C-N
42	606w		610vw	616	1.13	14.29	γ C-C-N
43	559m		558vw	541	3.54	20.55	β C-CH_3+ β C- NO_2
44	503s			472	12.13	13.88	β N4-C14
45			393vw	407	0.59	26.21	ρ $C17H_2$
46				374	2.32	30.50	β N4-C14
47			356vw	350	3.43	25.71	β C- CH_3 + γ C4-C14
48			280w	286	3.67	33.15	γ C- CH_3+ γ N-C-C
49				254	6.03	21.50	γ N-C-N+ γ O-H
50			226w	223	101.93	82.28	γ O-H
51			185w	212	3.71	23.23	β C- CH_3+ β C- NO_2
52				158	13.53	87.20	γ C-N-C + γ C-C17
53			132w	142	0.25	25.33	τ C- CH_3
54			106vw	105	2.47	41.33	γ C- CH_3+ γ C- NO_2
55			85vw	95	1.15	57.28	τ C- NO_2
56			74w	71	0.09	565.00	τ NO_2+ τ C4-C14
57				50	1.31	847.00	τ NO_2

IR_{int} - IR intensity; $Kmmol^{-1}$ Ra_{Int} – Raman Intensity, arb units; w-weak ; vw- very weak ; s-strong ; vs-very strong ; m-medium; br, sh- broad, shoulder ; υ - stretching; $υ_{sym}$ – symmetric stretching ; $υ_{asy}$- asymmetric stretching ; β- in plane bending ; γ- out-of –plane bending ; ω – wagging ; t- twisting ; δ –scissoring ; τ- torsion, ρ-rocking.

The theoretically computed wavenumber of O-H out-of-plane bending vibration which is at 223 cm^{-1} (Mode no. 50) method shows excellent agreement with FT-Raman recorded value at 226 cm^{-1}.

3.4.2. C-H vibrations

It is easy to assign the C-H stretching vibration for the title molecule because it has only one C-H stretching unit in the imidazole ring i.e. C2-H5 unit. The hetero aromatic structure shows the presence of C-H stretching vibration in the region 3100-3000 cm^{-1} which is the characteristic region for the ready identification of C-H stretching vibration [28]. In this region the bands are not affected appreciably by the nature of the substituents. The scaled vibration (Mode no. 2) by B3LYP method predicted at 3157 cm^{-1} shows a moderate agreement with the literature data [30]. This absorption is in good agreement with the calculated ones as far as frequencies, intensities are concerned. The same behavior was also found in *N*-methylpyrazole [30].

In the in-plane and out-of plane deformation vibration normally observed in the region 1300-750 cm^{-1}, the bands are sharp but are weak to medium intensity. The C-H in-plane bending vibration is computed at 1131 cm^{-1} (Mode no. 28) by B3LYP method. The recorded FT-IR / FT-Raman spectrum does not show any such band. The theoretically computed wavenumber at 860 cm^{-1} (Mode no. 35) by B3LYP method is assigned to C-H out-of-plane bending vibration which exactly

correlates well with FT-IR band at 864 cm^{-1} and FT-Raman band at 863 cm^{-1}.

3.4.3. CH_2 group vibrations

For the assignments of CH_2 group frequencies, basically six fundamentals can be associated to each CH_2 group namely, CH_2 sym-symmetric stretch, CH_2-asym, asymmetric stretch, CH_2 scis, scissoring and CH_2 rock, rocking modes which belong to in-plane vibrations of A' species. In addition to that CH_2 wag, wagging and CH_2 twist, twisting modes of CH_2 group would be expected to be out-of-plane bending vibrations of A'' species.

The C-H stretching vibrations of the methylene group are at lower frequencies than those of the aromatic C-H ring stretching. The asymmetric CH_2 stretching vibration is generally observed in the region 3000-2900 cm^{-1}, while the CH_2 symmetric stretch will appear between 2900-2800 cm^{-1} [31,32]. The CH_2 asymmetric and symmetric stretching vibrations computed by B3LYP method at 3059 and 2911 cm^{-1} (Mode nos. 3 and 8) are assigned to CH_2 asymmetric stretching modes of C14-H_2 and C17-H_2 units. The bands at 2983, 2885 cm^{-1} in FT-Raman spectrum are assigned to CH_2 symmetric stretching vibrations. The band at 3100 cm^{-1} as a medium band is assigned to CH_3 asymmetric stretching vibration. The theoretically computed wavenumbers at 2987 and 2878 cm^{-1} (Mode nos. 5 and 9), show excellent agreement with the experimental data.

In the present assignment, the CH_2 bending modes follow, in decreasing wavenumber, the general order CH_2 deformation > CH_2 wagging > CH_2 twist > CH_2 rock. Since the bending modes involving hydrogen atom attached to the central carbon falls into the 1450-875 cm^{-1} range there is extensive vibrational coupling of these modes with CH_2 deformations particularly with the CH_2 twist. It is notable that both CH_2 scissoring and CH_2 rocking were sensitive to the molecular conformation. For cyclohexane, the CH_2 scissoring mode has been assigned to the medium intensity IR band at about 1450 cm^{-1} [33]. The CH_2 deformation band which comes near 1463 cm^{-1} in alkenes [34] is lowered about 1440 cm^{-1} when the CH_2 group is next to a double or triple bond. A carbonyl, nitrile or nitro group each lowers the wavenumber of the adjacent CH_2 group [35] to about 1425 cm^{-1}. In our title molecule the scaled vibrational frequencies computed by B3LYP method at 1468 and 1424 cm^{-1} (Mode nos. 12 and 16) are assigned to CH_2 scissoring modes of C17-H_2 and C14-H_2 units which show good correlation with recorded spectrum at 1473 cm^{-1} in FT-IR, 1467 cm^{-1} in FT-Raman spectrum. The computed wavenumber by B3LYP method at 1409 and 1345 cm^{-1} (Mode nos. 17 and 21) are assigned to CH_2 wagging vibration of C17-H_2 and C14-H_2 units. The CH_2 twisting vibrations observed as a strong band in FT-IR spectrum at 1265 cm^{-1} and 1268 cm^{-1} as a very strong band in FT-Raman spectrum are assigned to CH_2 twisting vibrations. The theoretically computed wavenumber by B3LYP method at 1263 and 1227 cm^{-1} (Mode nos. 23 and 25) exactly correlates with experimental observations. The CH_2 rocking vibrations computed by B3LYP method show good agreement with experimental observations.

3.4.4. NO_2 vibrations

The molecule with NO_2 group possesses NO_2 asymmetric stretching vibration band in the range 1625-1540 cm^{-1} and that of the symmetric stretching vibration in the range 1400-1360 cm^{-1} [36]. The medium strong FT-IR band at 1535 cm^{-1} and 1533 cm^{-1} as a very strong band in FT-Raman spectrum are assigned to NO_2 asymmetric stretching vibration for MTD molecule, the theoretically computed wavenumber at 1544 cm^{-1} (Mode no. 10) as a strong intensity shows good correlation with experimental data as shown in Table 3. The symmetric NO_2 stretching vibration computed by B3LYP method at 1342 cm^{-1} (Mode no. 22), also shows good agreement with literature data [35], but the recorded spectrum does not show any kind of band in this region.

Aromatic nitro compounds have a band of weak-to-medium intensity in the region 590-500 cm^{-1} [35] due to the in-plane deformation mode of NO_2 group. In our present study, the medium and very weak band in FT-IR at 559 cm^{-1} and FT-Raman spectrum at 558 cm^{-1} are assigned to C-NO_2 in-plane-bending vibration. The theoretically computed wavenumber at 541 cm^{-1} support the experimental wavenumber at 558 cm^{-1} (Mode no. 43). The out-of-plane deformation vibrations have a weak to medium absorption band in the region 775-662 cm^{-1} [35]. The theoretically computed wavenumber at 853 cm^{-1} (Mode no. 36) is assigned to C-NO_2 out-of-plane-bending vibration.

The deformation vibrations of NO_2 group (scissoring, wagging, rocking and twisting) contribute to several normal modes in the low frequency region. The NO_2 scissoring [35] occurs in the region 805 ± 60 cm^{-1}. For nitrobenzene [35], δNO_2 is reported at 852 cm^{-1}, for $H_2C{=}CHNO_2$ at 890 cm^{-1} and for 1,3-dinitrobenzene at 904 and 834 cm^{-1}. In our present study a very strong band in FT-IR and weak band in FT-Raman spectrum at 826 and 828 cm^{-1} are assigned to NO_2 scissoring mode. The theoretical computed wavenumber for this mode is at 818 cm^{-1} (Mode no. 37).

In aromatic compounds the wagging mode (ωNO_2) is assigned at 740±50 cm^{-1} with a moderate to strong intensity, a region in which γCH is also active [35], ωNO_2 is reported at 701 and 728 cm^{-1} for 1,2-dinitrobenzene and at 710 and 772 cm^{-1} for 1,4-dinitrobenzene. In the present study the medium band in FT-IR and FT-Raman spectrum at 744 and 737 cm^{-1}, respectively, are assigned to wagging mode NO_2 group, the computed vibrational mode for this vibration at 730 cm^{-1} is also in good agreement with experimental observation (Mode no. 38). The other vibration computed by B3LYP method shows good agreement with experimental observation as shown in Table 3.

3.4.5. Methyl group vibrations

The title molecule MTD under consideration possesses one CH_3 group. For the assignments of CH_3 group frequencies one can expect nine fundamentals which can be associated to each CH_3 group, namely the symmetrical stretching in CH_3 (CH_3 sym.stretch) and asymmetrical stretching (CH_3 asy. stretch), in-plane stretching modes (i.e. in plane hydrogen stretching mode); the symmetrical (CH_3 sym. deform) and asymmetrical (CH_3 asy deform) deformation modes; the in-plane rocking (CH_3 ipr) out-of-plane rocking (CH_3 opr) and twisting ($t$$CH_3$) bending modes. Methyl groups are generally referred to as electron donating substituents in the aromatic ring system. The methyl hydrogen atoms in EDP are simultaneously subjected to hyperconjucation and backdonation, which causes the decrease of stretching wavenumbers and infrared intensities, as reported in literature [31] for similar molecular system.

In the spectra of methyl esters the overlap of the region in which both asymmetric stretching [35] $\nu_{as}CH_3$ absorb with a weak to medium intensity (2985±25 cm^{-1} and 2970±30 cm^{-1}) is not large and regularly seen above 3000 cm^{-1}. The computed wavenumber of modes corresponding to $\nu_{as}CH_3$ group is 3039 and 2975 cm^{-1}. In this mode two C-H bonds of the methyl group are extending while the third one is contracting. For the title compound, the bands at 3019 cm^{-1} in the FT-Raman spectrum is assigned to as methyl asymmetric stretching modes. The symmetric stretching mode $\nu_{sy}CH_3$ is expected in the range 2920±80 cm^{-1} in which all three C-H bonds extend and contract in-phase [35]. The band seen at 2936 cm^{-1} (Raman) and 2929 cm^{-1} (DFT) is assigned to this mode.

For the methyl substituted benzene derivatives the asymmetric and symmetric deformation vibrations of methyl

group normally appear in the region 1465-1440 cm^{-1} and 1390-1370 cm^{-1}, respectively [28,37-39]. Based on the above literature data, in our present study the weak band observed in FT-Raman spectrum at 1435 and 1377, 1355 cm^{-1} are assigned to CH_3 asymmetric and symmetric deformation vibration. The theoretically computed value by B3LYP method show good agreement with literature as well as experimental observations.

The rocking vibrations of CH_3 group unit appear as independent vibrations. These modes usually appear [40] in the region 1070-1010 cm^{-1}. In the present study, the FT-Raman spectrum at 990 cm^{-1} is assigned to CH_3 rocking vibration. The theoretically computed value at 1027 cm^{-1} (Mode no. 31) assigned to CH_3 rocking vibration coincides with literature as well as recorded FT-Raman spectrum. The CH_3 torsional vibrations are not observed in the FT-IR spectrum because these appear at very low frequency. The FT-Raman experimental observations at 132 cm^{-1} show good agreement with computed wavenumber at 142 cm^{-1}. This means that the rotation of the methyl group is not significantly hindered. The CH_3 stretching and in-plane and out-of-plane bending vibration computed by B3LYP method also shows good agreement with experimental observations as shown in Table 3.

3.4.6. Ring vibrations (C-N, C=N vibrations)

The C=N stretching skeletal bands [41,42] are observed in the range 1650-1550 cm^{-1}. For conjugated azines, the νC=N mode is reported [43] at 1553 cm^{-1}. For the title compound the band observed at 1486 cm^{-1} as a very strong band in the FT-Raman is assigned to this mode. The DFT calculations give this mode at 1503 cm^{-1} (Mode no. 11). Mangalam and Kurup [44] reported νC=N in the range 1571-1602 cm^{-1}, for thio semicarbazone ligands. El-Asmy and Al-Hazmi [45] reported νC=N in the range 1606-1627 cm^{-1} for benzophenone-substituted semicarbazones. The C-N stretching vibration [35] coupled with the δN-H, is moderately active in the region 1275 ± 55 cm^{-1}. El.Shahawy et al [46] observed a band at 1320 cm^{-1} in the IR spectrum as this νC-N mode. The DFT calculations give the corresponding band at 1345 cm^{-1} (Mode no. 21). However the experimental observation does not support this kind of band.

3.5. UV-spectral analysis

All the structures allow strong π-π* or σ-σ* transition in the UV-vis region with high extinction coefficients. Natural bond orbital analysis indicates that molecular orbitals are mainly composed of σ atomic orbital, so the above electronic transitions are mainly derived from the contribution of σ-σ* bands. The UV-vis absorption spectrum of the sample in ethanol is shown in Figure 5. On the basis of fully optimized ground-state structure, TD-DFT/B3LYP/6-311G(d,p) calculations have been used to determine the low-lying excited states of MTD. The calculated results involving the vertical excitation energies, oscillator strength (f) and wavelength are carried out and compared with the measured experimental wavelength. Typically, according to Frank-Condon principle, the maximum absorption peak (λ_{max}) correspond in an UV-Visible spectrum to vertical excitation. TD-DFT/B3LYP predict that one intense electronic transition at (380 nm) with an oscillator strength f=0.000, shows good agreement with measured experimental data (λ_{exp} = 401 nm) The HOMO represents the ability to donate an electron, LUMO as an electron acceptor represents the ability to obtain an electron. The HOMO and LUMO energy calculated by B3LYP method is shown below. This electronic absorption corresponds to the transition from the ground to the first excited state and is mainly described by one electron excitation from the highest occupied molecular orbital (HOMO) to the lowest unoccupied molecular orbital (LUMO). Energy difference between HOMO and LUMO analysis is called as energy gap that is an important stability for structures.

The HOMO is located over the imidazole ring, the HOMO → LUMO transition implies an electron density transfer to NO_2 from imidazole ring. Moreover, these orbital significantly overlap in their position for MTD. The atomic orbital compositions of the frontier molecular orbital are sketched in Figure 7.

HOMO energy (B3LYP) = 6.4284 eV
LUMO energy (B3LYP) = 4.3843 eV
HOMO–LUMO energy gap (B3LYP) = 2.0441 eV

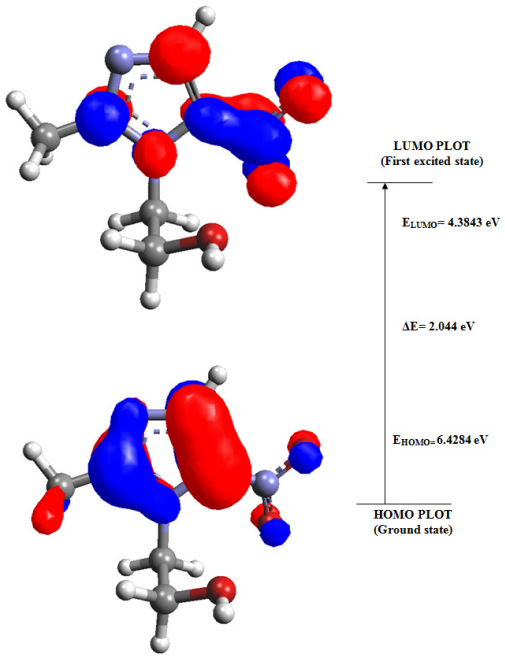

Figure 7. The atomic orbital compositions of the frontier molecular orbital for metronidazole.

The calculated self-consistent field (SCF) energy of MTD is -624.03782 a.u. Moreover lower the HOMO and LUMO energy gap explains the eventual charge transfer interactions taking place within the molecule.

3.6. NMR analysis

The isotropic chemical shifts are frequently used as an aid in identification of reactive organic as well as ionic species. It is recognized that accurate predictions of molecular geometries are essential for reliable calculations of magnetic properties. Therefore, full geometry optimization of MTD were performed by using B3LYP/6-311G(d,p) method. Then, Gauge-Independent Atomic Orbital (GIAO) ^1H and ^{13}C chemical shift calculations of the compound has been made by same method.

Application of the GIAO [10,11] approach to molecular systems was significantly improved by an efficient application of the method to the ab initio SCF calculations, using techniques borrowed from analytic derivative methodologies. GIAO procedure is somewhat superior since it exhibits a faster convergence of the calculated properties upon extension of the basis set used. Taking into account the computational cost and the effectiveness of calculation, the GIAO method seems to be preferable from many aspects at the present state of this subject.

Table 4. Experimental and theoretical chemical shifts (^{13}C, ^{1}H) of MTD by B3LYP/6-311G(d,p) method [δ(ppm)].

Atom position	Experimental	B3LYP 6-311G(d)	Atom position	Experimental	B3LYP 6-311G(d)
C1	153.28	156.32	O12		-1649.99
C2	133.41	137.82	O13		-1676.48
C3	153.28	163.93	C14	48.7	41.72
N4		74.02	H15	3.78	4.49
H5	7.91	9.15	H16	3.78	4.69
N6		-67.34	C17	60.76	53.68
C7	13.96	4.98	H18	4.37	4.59
H8	2.37	2.564	H19	4.37	4.54
H9	2.37	2.5102	O20		290.77
H10	2.37	2.68	H21	4.64	2.89
N11		-331.81			

On the other hand, the density functional methodologies offer an effective alternative to the conventional correlated methods, due to their significantly lower computational cost.

The molecular structure of MTD is optimized by using B3LYP method. Then, gauge-independent atomic orbital (GIAO) ^{13}C and ^{1}H chemical shift calculations of the title compound is made by using B3LYP method. The ^{1}H and ^{13}C chemical shifts were measured in a less polar (DMSO) solvent. The result in Table 4 shows that the range ^{13}C NMR chemical shift of the typical organic molecule usually is >100 [47,48], the accuracy ensures reliable interpretation of spectroscopic parameters.

It is true from the above literature value, in our present study, the title molecule MTD also falls with the above literature data except with the methyl carbon and ethylene carbon atoms.

In the present paper, the signal observed at 153.28 ppm in ^{13}C NMR spectrum is assigned to C1 and C3 carbon atoms shows good agreement with calculated chemical shifts value of 156.32 and 163.93 ppm respectively as shown in Table 4.The H atom is the smallest of all atoms and mostly localized on the periphery of the molecules. Therefore their chemical shifts would be more susceptible to intermolecular interactions in the aqueous solution as compared with that of other heavier atoms. Another important aspect is that, hydrogen attached or nearby electron-withdrawing atom or group can decrease the shielding and move the resonance of attached proton towards a higher frequency. By contrast electron donating atom or group increases the shielding and moves the resonance towards a lower frequency. In this study, the chemical shifts obtained and calculated for the hydrogen atoms of methyl groups are quite low. All values are ≤ 3 ppm [48] due to the shielding effect. It is also true from above literature data in the present study the methyl protons at the C7 appears as a singlet with three proton integral at 2.37 ppm shows moderate agreement with computed shift at 13.96 ppm as shown in Table 4. Correlation graphics of calculated and experimental chemical shift for MTD molecule as shown in Figure 8.

4. Conclusion

In this study, the results of experimental and the DFT level of theory with 6-311G(d,p) basis set are reported. Computed and experimental geometric parameters, vibrational frequencies, chemical shifts and UV electronic properties of the title compound have been compared. The difference between the observed and scaled wavenumber values of the fundamentals are very small. However, the difference between the observed and scaled wavenumber values of O-H fundamental is very large, due to the fact that the presence of the intermolecular hydrogen bonds in the solid state which must be reflected in the IR spectra. Therefore, the assignments made at DFT level of theory with reasonable deviations from the experimental values seems to be correct. NBO result reflects the charge transfer mainly due to NO_2 group. The UV spectrum was measured in ethanol solution. The theoretically constructed FT-IR and FT-Raman spectrum shows good correlation with experimentally observed FT-IR and FT-Raman spectrum.

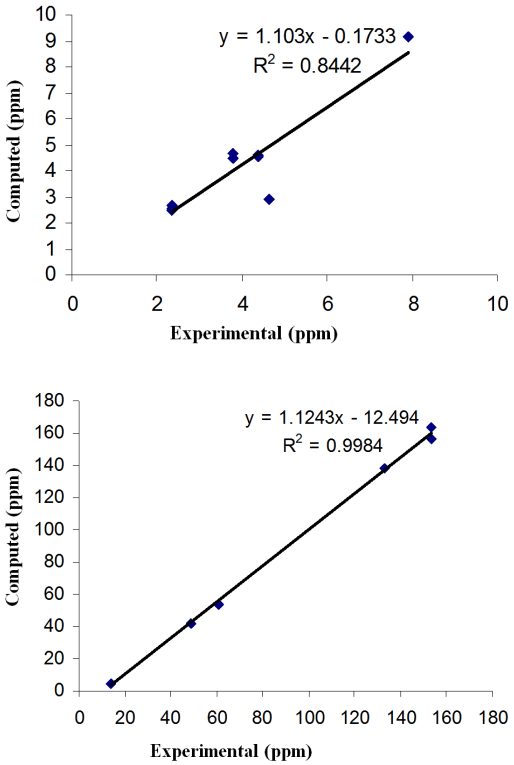

Figure 8. Correlation graphics of calculated and experimental chemical shift for metronidazole.

References

[1]. Burtin, P. *Am. J. Obstet. Gynecol.* **1995**, *172*, 525-529.
[2]. Lam, A.; Rivera, A.; Fuentes, G. R. *Microporous & Mesoporous Mater.* **2001**, *49*, 157-162.
[3]. Blaton, N. M.; Peetres, O. M.; Ranter, C. J. D. *Acta Cryst. B* **1979**, *35*, 2465-2467.
[4]. Sebastian, S.; Sundaragnesan, N.; Manoharan, S. *Spectrochim Acta A* **2009**, *74*, 312-323.
[5]. Abraham, J. P.; Joe, I. H.; George, V.; Nielson, O. F.; Jayakumar, V. S. *Spectrochim. Acta A* **2003**, *59*, 193-199.
[6]. Binoy, J.; Abraham, J. P.; Joe, I. H.; Jayakumar, V. S.; Aubard, J.; Nielson, O. F. *J. Raman Spectrosc.* **2005**, *36*, 63-72.
[7]. Gaussian 03, Revision A. 1, Frisch, M. J.; Trucks, G. W.; Schlegel, H. B.; Scuseria, G. E.; Robb, M. A.; Cheeseman, J. R.; Montgomery, Jr. J. A.; Vreven, T.; Kudin, K. N.; Burant, J. C.; Millam, J. M.; Iyengar, S. S.; Tomasi, J.; Barone, V.; Mennucci, B.; Cossi, M.; Scalmani, G.; Rega, N.; Petersson, G. A.; Nakatsuji, H.; Hada, M.; Ehara, M.; Toyota, K.; Fukuda, R.; Hasegawa, J.; Ishida, M.; Nakajima, T.; Honda, Y.; Kitao, O.; Nakai, H.; Klene, M.; Li, X.; Knox, J. E.; Hratchian, H. P.; Cross, J. B.; Adamo, C.; Jaramillo, J.; Gomperts, R.; Stratmann, R. E.; Yazyev, O.; Austin, A. J.; Cammi, R.; Pomelli, C.; Ochterski, J. W.; Ayala, P. Y.; Morokuma, K.; Voth, G. A.; Salvador, P.; Dannenberg, J. J.; Zakrzewski, V. G.; Dapprich, S.; Daniels, A. D.; Strain, M. C.; Farkas, O.; Malick, D. K.; Rabuck, A. D.;

Raghavachari, K.; Foresman, J. B.; Ortiz, J. V.; Cui, Q.; Baboul, A. G.; Clifford, S.; Cioslowski, J.; Stefanov, B. B.; Liu, G.; Liashenko, A.; Piskorz, P.; Komaromi, I.; Martin, R. L.; Fox, D. J.; Keith, T.; Al-Laham, M. A.; Peng, C. Y.; Nanayakkara, A.; Challacombe, M.; Gill, P. M. W.; Johnson, B.; Chen, W.; Wong, M. W.; Gonzalez, C.; Pople, J. A. Gaussian, Inc. , Pittsburgh PA, 2003.

[8]. Schlegel, H. B. *J. Comput. Chem.* **1982**, *3*, 214-218.

[9]. Frisch, A.; Nielson, A. B.; Holder, A. J. GAUSSVIEW User Manual, Gaussian Inc., Pittsburgh, PA, 2000.

[10]. Glendening, E. D.; Reed, A. E.; Carpenter, J. E.; Weinhold, F. NBO version 3. 1, TCI, University of Wisconsin, Madison, 1998.

[11]. Ditchfield, R. *Mol. Phys.* **1974**, *27*, 789-807.

[12]. Wolinski, K.; Hinton, J. F.; Pulay, P. *J. Am. Chem. Soc.* **1990**, *112(23)*, 8251-8260.

[13]. Azizi, N.; Rostami, A. A. , Godarzian, A. *J. Phys. Soc. Jpn*. **2005**, *74*, 1609-1620.

[14]. Rohlfing, M.; Leland, C.; Allen. C.; Ditchfield, *R. Chem. Phys.* **1984**, *87*, 9-12.

[15]. Keresztury, G.; Holly, S.; Varga, J.; Besenyei, G.; Wang , A. Y; Durig, J. R. *Spectrochim. Acta A* **1993**, *49*, 2007-2026.

[16]. Keresztury, G.; Chalmers, J. M.; Griffith, P. R. (Eds.), Raman Spectroscopy: Theory, in Hand book of Vibrational Spectroscopy, Vol. 1, John Wiley & Sons Ltd., New York, 2002.

[17]. Sundaraganesan, N.; Ilakiamani, S.; Saleem, H.; Wojciechowski, D. M.; Michalska, D. *Spectrochim Acta A* **2005**, *61*, 2995-3001.

[18]. Jaffrey, G. A. An Introduction to Hydrogen Bonding, Oxford University Press, 1997.

[19]. Szafran, M.; Komasa, A.; Adamska, E. B. *J. Mol. Struct. (THEOCHEM)* **2007**, *827*, 101-107.

[20]. James, C.; Amal Raj, A.; Reghunathan, R.; Joe, I. H.; Jayakumar, V. S. *J. Raman Spectrosc.* **2006**, *37*, 1381-1392.

[21]. Na, L. J.; Rang, C. Z.; Fang, Y. Z. *J. Zhejiang Univ. Sci. B* **2005**, *6*, 584-589.

[22]. Pulay, P.; Forgarasi, G.; Ponger, G.; Boggs, J. E.; Vargha, A. *Am. Chem. Soc.* **1983**, *105*, 7037-7047.

[23]. Scott, A. P.; Radom, L. *J. Phys. Chem.* **1996**, *100*, 16502-16513.

[24]. Michalska, D.; Bienko, D. C.; Bienko, A. J. A.; Latajaka, Z. *J. Phys. Chem.* **1996**, *100*, 1186-1193.

[25]. Marshal, J. *Ind. J. Phys. B* **1998**, *72*, 661-667.

[26]. Lutz, E. T. G.; Mass, J. H. V. *Spectrochim. Acta* A **1986**, *42*, 749-755.

[27]. Sundaraganesan, N.; Saleem, H.; Mohan, S. *Spectrochim. Acta A* **2003**, *59*, 2511-2517.

[28]. Varsanyi, G. Assignments for Vibrational Spectra of Seven Hundred Benzene Derivatives, Vol. 1 and 2, Academic Kiado: Budapest, 1973.

[29]. Sadekov, I. D. *Rus. Chem. Rev.* **1970**, *30*, 179-195.

[30]. Orza, J. M.; Obilia, M. O.; Yanez, M. J.; Elguero, *Spectrochim Acta*. *A* **1997**, *53*, 1383-1398.

[31]. Sajan, D.; Binoy, J.; Pradeep, B.; Krishnan, K. V.; Kartha, V. B.; Joe, I. H.; Jayakumar, V. S. *Spectrochim. Acta A* **2004**, *60*, 173-180.

[32]. Furic, K.; Mohack, V.; Bonifacic, M.; Stefanic, I. *J. Mol. Struct.* **1992**, *267*, 39-44.

[33]. Wiberg, K. B.; Sharke, A. *Spectrochim. Acta A* **1973**, *29*, 583-594.

[34]. Mc, Murry, H. L.; Thornton, V. *Anal. Chem.* **1952**, *24*, 318-329.

[35]. Roeges, N. P. G, A Guide to the Complete Interpretation of Infrared Spectra of Organic Structures, Wiley, New York, 1994.

[36]. Lakshmaiah, B.; Ramana Rao, G. *J. Raman Spectrosc.* **1989**, *20*, 439-448.

[37]. Areanas, J. F.; Lopez Tocon, I.; Otero, J. C.; Marcos, J. I. *J. Mol. Struct.* **1997**, *410*, 433-446.

[38]. Lopez Tocon, I.; Wooley, M. S.; Otero, J. C.; Marcos, J. I. *J. Mol. Struct.* **1997**, *410*, 447-450.

[39]. Areanas, J. F.; Lopez Tocon, I.; Wooley, M. S.; Otero, J. C. Marcos, J. I. *J. Chem. Soc. Faraday Trans. II* **1988**, *84*, 53-65.

[40]. Silverstein, M.; Basseler, G. C.; Morill, C. Spectrometric Identification of Organic Compounds, Wiley, New York, 1981.

[41]. Yalcin, I.; Sener, E.; Ozden, O.; Akin, O. *Eur. J. Med. Chem.* **1990**, *25*, 705-708.

[42]. Saxena, R.; Kandpaul, L. D.; Mathur, G. N, *Polym. Sci. A* **2002**, *40*, 3951-3959.

[43]. Panicker, C. Y.; Varghese, H. T.; Ambujakshan, K. R.; Mathew, S.; Ganguli, S.; Nanda, A. K; Alsenoy, C. V.; Mary. S. Y. *J. Mol. Struct.* **2010**, *963*, 137-144.

[44]. Mangalam, N. A.; Kurup, M. R. P. *Spectrochim. Acta A* **2009**, *71*, 2040-2044.

[45]. El Asmy, A. A.; Al Hazmi, G. A. A. *Spectrochim. Acta A* **2009**, *71*, 1885-1890.

[46]. El Shahawy, Ahmed, S. M.; Sayed, N. K. *Spectrochim. Acta A* **2007**, *66*, 143-153.

[47]. Kalinowski, H. O.; Berger, S.; Brawn, S. Carbon ^{13}NMR spectroscopy, John Wiley and Sons, Chichester, 1988.

[48]. Pihlajer, K.; Kleinpeter, E. (EDS), Carbon ^{13}Chemical shifts in Structure and Spectrochemical Analysis, VCH publishers, Deerfield Beach, 1994.